Correction of Errors in Polarization Based Dynamic Phase Shifting Interferometers

Bradley Kimbrough

4D Technology Corporation, Tucson Arizona
brad.kimbrough@4dtechnology.com

1 Introduction

Polarization based interferometers for single snap-shot measurements allow single frame, quantitative phase acquisition for vibration insensitive measurements of optical surfaces and have been successfully used on a variety of interferometer types. This technique generally involves the simultaneous acquisition of three or more images on the same camera or multiple cameras, which are phase shifted by polarization. Examples of these types of systems would include the multiple camera system of Smythe and Moore [1], and more recently, systems utilizing a micro-polarizer phase mask [2] on a single camera.

Application of these polarization based phase sensors requires the test and reference beams of the interferometer to be orthogonally polarized. As with all polarization based interferometers, these systems can suffer from phase dependent errors resulting from systematic polarization aberrations; this is especially true in high numerical aperture systems. This type of measurement error presents a particular challenge because it varies in magnitude both spatially and temporally between each measurement. It typically manifests as "fringe print-through" where a small component of the intensity fringe pattern appears in the measured surface. In this paper, a general discussion of phase calculation error presented. We then present an algorithm that is capable of mitigating phase-dependent measurement error on-the-fly. The algorithm implementation is non-iterative providing sensor frame rate limited phase calculations. Finally, results are presented for both a high numerical aperture system, where the residual error is reduced to the shot noise limit, and a system with significant birefringence in the test arm.

2 General Phase Calculation Errors

Regardless of the technique, all phase calculation processes ultimately return a phase value which is computed as the arctangent of the ratio of two values. These two values will be referred to as the numerator, N, and the denominator, D, terms. Each of these terms is a function of the actual phase value, θ, being measured, and is generally calculated from a set of measured interferograms. The simple relationship between the calculated phase, $\theta\hat{}$, and N and D is shown in Eq. 1.

W. Osten (ed.), *Fringe 2013*,
DOI: 10.1007/978-3-642-36359-7_11,

$$Tan(\theta') = N(\theta)/D(\theta) \tag{1}$$

A general expression for N and D is given in Eq. 2 and 3.

$$N(\theta) = y_o + a_y Sin(\theta + \phi_y) \tag{2}$$

$$D(\theta) = x_o + a_x Cos(\theta + \phi_x) \tag{3}$$

Together, Eq. 2 and 3 are the parametric equations for a general ellipse where each {x, y} point on the ellipse is given by $\{D, N\}$. The phase calculation process is error free if the following condition holds for all values of calculated phase:

$$\theta' = \theta + \theta_o \tag{4}$$

where θ_o is a constant. In order for equation 4 to be true, the following conditions must be met:

$$x_o = 0 \quad and \quad y_o = 0, \quad a_x = a_y, \quad \phi_x = \phi_y \tag{5}$$

Simply put, the N and D terms must not have any offset, the amplitudes must be equal and the phase must be in quadrature. Associating the $\{D, N\}$ values with $\{x, y\}$ coordinate pairs, the conditions for error free phase calculation are seen to be the requirements that all $\{D, N\}$ coordinate pairs fall on a circle centered at the origin, with amplitude $r = a_x = a_y$. In general, however, due to unavoidable errors in the phase calculation process, all $\{D, N\}$ coordinate pairs will fall on an ellipse centered at $\{x_o, y_o\}$. The error in the phase calculation is equal to the difference between the parameterizing angle, θ, and the coordinate angle, θ'. The relationship between the parameterizing angle and the coordinate angle for a general ellipse is shown in figure 1.

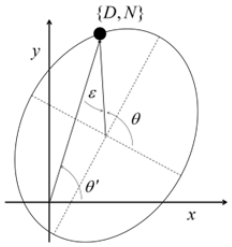

Fig. 1 General ellipse plot showing the parametric angle, θ, the coordinate angle, θ', and the difference angle, $\varepsilon = \theta' - \theta$, for a given point $\{D, N\}$

The parameter angle is always equal to the coordinate angle in a circle centered at the origin; this is not the case for a non-centered circle or an ellipse, resulting in the well known single and double frequency print through errors. Lissajous curves are created by plotting the $\{D, N\}$ coordinate pairs as defined in Eq. 2 and 3.

Three different curves were created corresponding to an offset error, and amplitude error, and a phase error. These curves are shown in figure 2a. For each of the curves given in figure 1, the difference between the parametric angle, θ, and the coordinate angle, $\theta^{\wedge}$, at each point is plotted in figure 2b. Generally, offset, amplitude and phase errors occur simultaneously, and the phase calculation error will be a non-linear combination of these three error sources.

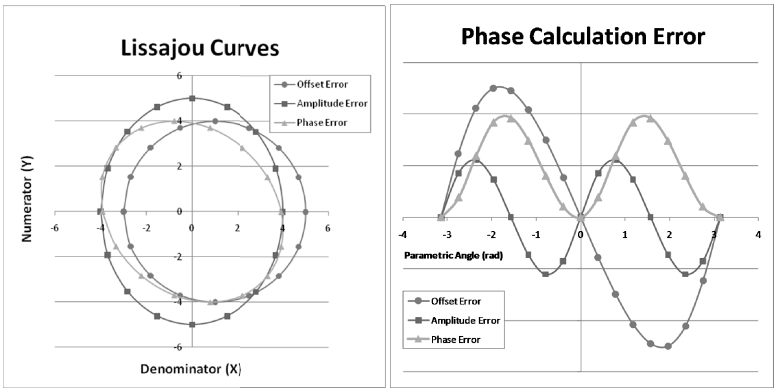

Fig. 2 A. Lissajous plots associated with offset, amplitude, and phase errors where coordinate points given by parametric Eq. 2 and 3. B. Phase calculation error given by the difference between the coordinate and parametric angle of each point in the curves of figure 2a.

The use of Lissajous curves in the analysis of phase shifting interferometry has been discussed by Kinnstaetter et al. [3], who utilizes Lissajous figures in the analysis of systematic errors; intensity variation, reference phase errors, vibrations, and nonlinearities of the photo detector. Farrell and Player utilize ellipse fitting and Lissajous figures to calculate the phase difference between interferograms. [4] The idea of using the calculated bias, offset, and phase shift to correct the measured fringe fields which are then used in standard phase shifting calculations is also presented in their paper.

3 Ellipse Fitting and Measurement Transformation

Ignoring a constant phase offset and setting φ= (φy-φx), equations 2 and 3 may be written as:

$$N(\theta) = y_o + a_y Sin(\theta + \phi) \tag{6}$$

$$D(\theta) = x_o + a_x Cos(\theta) \tag{7}$$

Equations 6 and 7 describe a general ellipse with offset {xo, yo}, and semi-major and minor amplitudes of {ax, ay}. The ellipse orientation angle, α, referenced to the x-axis is given by:

$$Tan(2\alpha) = \frac{2a_x a_y Sin(\phi)}{a_x^2 - a_y^2} \tag{8}$$

The parametric coefficients, {xo, yo, ax, ay, φ} may be determined through fitting the Lissajous curves shown in figure 2 to a general ellipse. Using the best fit ellipse parameters, the measurement {*D*, *N*} points are transformed to lie on a circle centered at the origin. In other words, the measured parameters are used to remove the offsets, equalize amplitudes and orthogonalize the *N* and *D* terms. This transformation is shown in equation 9, where *R* is the rotation matrix.

$$\{D_t, N_t\} = R(-\alpha) \cdot \{1, \tfrac{a_x}{a_y}\} \cdot R(\alpha) \cdot \{D - x_o, N - y_o\} \tag{9}$$

A series of phase measurements, >5, are made where the average phase is dithered between 0 and 2pi radians. For each measurement field point, the series of {*D*, *N*} pairs are fit to a general ellipse, the parametric coefficients are determined, and finally, the quadrature points are transformed to lie on a circle centered at the origin. These transformed {*D*, *N*} pairs are then use to calculate the error free phase.

4 Measurement Results

One advantage of using the pixelated polarization mask phase sensor is that the mechanisms leading to phase-dependent measurement error are static for a given test setup, and thus it is possible to correct for them. The dominate mechanism is polarization mixing between the test and reference beams which is caused by birefringence in both the common and non-common path portions of the interferometer. For a given test setup the polarization mixing is static, although it may not be spatially uniform, thus by using the procedure of section 3 it is possible to measure and correct for the error on a pixel by pixel basis.

4.1 High Numerical Aperture System Measurement

In terms of the discussion of section 1, polarization mixing primarily results in offset terms in the numerator and denominator of Eq. 1 and 2 giving single frequency print-through in the phase measurement. There is also a change in the amplitude balance which results in a lower amplitude double frequency print-through error. Figure 3 shows the results of a single phase measurement on a super smooth flat (surface roughness <0.1nm RMS). As can be seen, the standard measurement procedure results in about 15nm (λ/50) of single frequency print through. If a flat field calibration procedure is used, which is roughly equivalent to

normalizing the offset coefficients, the single frequency print-through is mostly eliminated, but a double frequency component with 3nm peak-to-valley remains. Application of the full phase correction process of section 3 results in near elimination of both single and double frequency print-through giving a 0.3 nm (λ/2000) peak-to valley error which is below the shot noise limit. Note that these are single shot, not averaged measurements.

4.2 Low Numerical Aperture System with Significant Birefringence Measurement Results

A measurement posing a significant challenge to polarization control was the test of a 0.75-meter diameter convex hyperboloid with a conic constant of -1.660 and radius of curvature of 1.780 meters. This mirror was cryo-tested at 30K using an aspheric test plate. A 4D Fizcam2000 was used to measure the interferogram generated by the wavefront reflected from the secondary mirror and the aspheric test plate. [5]

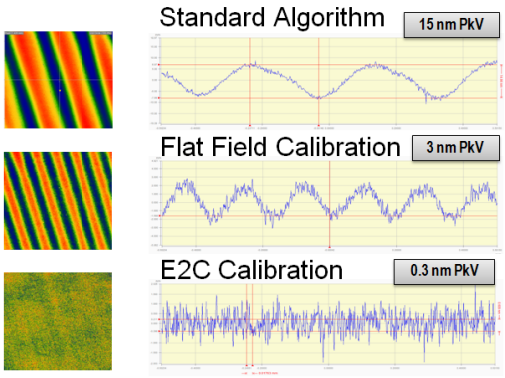

Fig. 3 Comparison of phase calculation errors for a high numerical aperture system

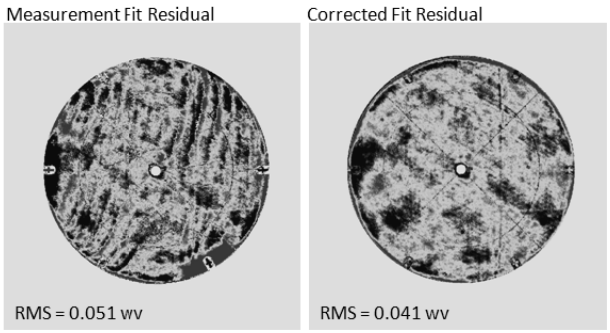

Fig. 4 Print-through correction on a cryo-tested convex hyperboloid. Measurement residuals resulting from the removal of a 32 term Zernike fit shown.

Use of this challenging arrangement resulted in significant polarization aberration in the beams returning to the interferometer. As a result, there was a significant amount of print-through error in the uncorrected phase measurement. Fig. 4 shows both the uncorrected and corrected residual phase maps resulting from the removal of a 32 term Zernike fit. As can be seen, print through error is no longer evident and the residual wavefront has gone from 0.051 to 0.041 waves RMS.

5 Summary

Polarization based instantaneous phase measurement systems can suffer from phase dependent errors resulting from systematic polarization aberrations. A general discussion of phase shifting calculation errors has been provided along with a phase error correction methodology. Finally, two examples of phase measurement correction have been shown.

References

1. Smythe, R., Moore, R.: Instantaneous Phase Measuring Interferometry. Opt. Eng. 23, 361–364 (1984)
2. Millerd, J.E., Wyant, J.C.: Simultaneous phase-shifting Fizeau interferometer. US Patent 7,230,718 (2007)
3. Kinnstaetter, K., Lohmann, A.W., Schwider, J., Streibl, N.: Accuracy of phase shifting interferometry. Appl. Opt. 27, 5082–5089 (1988)
4. Farrell, C.T., Player, M.A.: Phase step measurement and variable step algorithms in phase-shifting interferometry. Meas. Sci. Technol. 3, 953 (1992)
5. Stahl, H.P., et al.: Survey of interferometric techniques used to test JWST optical components. In: Proc. SPIE 7790, Interferometry XV: Techniques and Analysis, p. 779002 (2010)